EUROPEAN ORGANIZATION FOR NUCLEAR RESEARCH

CERN-PH-EP/2007-025
OPAL PR423
9 July 2007

Bose-Einstein study of position-momentum correlations of charged pions in hadronic Z^0 decays

The OPAL Collaboration

Abstract

A study of Bose-Einstein correlations in pairs of identically charged pions produced in e^+e^- annihilations at the Z^0 peak has been performed for the first time assuming a non-static emitting source. The results are based on the high statistics data obtained with the OPAL detector at LEP. The correlation functions have been analyzed in intervals of the average pair transverse momentum and of the pair rapidity, in order to study possible correlations between the pion production points and their momenta (position-momentum correlations). The Yano-Koonin and the Bertsch-Pratt parameterizations have been fitted to the measured correlation functions to estimate the geometrical parameters of the source as well as the velocity of the source elements with respect to the overall centre-of-mass frame. The source rapidity is found to scale approximately with the pair rapidity, and both the longitudinal and transverse source dimensions are found to decrease for increasing average pair transverse momenta.

(Submitted to Eur. Phys. J. C)

The OPAL Collaboration

G. Abbiendi[2], C. Ainsley[5], P.F. Akesson[7], G. Alexander[21], G. Anagnostou[1], K.J. Anderson[8], S. Asai[22], D. Axen[26], I. Bailey[25], E. Barberio[7,p], T. Barillari[31], R.J. Barlow[15], R.J. Batley[5], P. Bechtle[24], T. Behnke[24], K.W. Bell[19], P.J. Bell[1], G. Bella[21], A. Bellerive[6], G. Benelli[4], S. Bethke[31], O. Biebel[30], O. Boeriu[9], P. Bock[10], M. Boutemeur[30], S. Braibant[2], R.M. Brown[19], H.J. Burckhart[7], S. Campana[4], P. Capiluppi[2], R.K. Carnegie[6], A.A. Carter[12], J.R. Carter[5], C.Y. Chang[16], D.G. Charlton[1], C. Ciocca[2], A. Csilling[28], M. Cu ani[2], S. Dado[20], G.M. Dallavalle[2], A. De Roeck[7], E.A. De Wolf[7,s], K. Desch[24], B. Dienes[29], J. Dubbert[30], E. Duchovni[23], G. Duckeck[30], I.P. Duerdoth[15], E. Etzion[21], F. Fabbri[2], P. Ferrari[7], F. Fiedler[30], I. Fleck[9], M. Ford[15], A. Frey[7], P. Gagnon[11], J.W. Gary[4], C. Geich-Gimbel[3], G. Giacomelli[2], P. Giacomelli[2], M. Giunta[4], J. Goldberg[20], E. Gross[23], J. Grunhaus[21], M. Gruwe[7], A. Gupta[8], C. Hajdu[28], M. Hamann[24], G.G. Hanson[4], A. Harel[20], M. Hauschild[7], C.M. Hawkes[1], R. Hawkings[7], G. Herten[9], R.D. Heuer[24], J.C. Hill[5], D. Horvath[28,c], P. Igo-Kemenes[10], K. Ishii[22], H. Jeremie[17], P. Jovanovic[1], T.R. Junk[6,i], J. Kanzaki[22,u], D. Karlen[25], K. Kawagoe[22], T. Kawamoto[22], R.K. Keeler[25], R.G. Kellogg[16], B.W. Kennedy[19], S. Kluth[31], T. Kobayashi[22], M. Kobel[3,t], S. Komamiya[22], T. Kramer[24], A. Krasznahorkay Jr.[29,e], P. Krieger[6,l], J. von Krogh[10], T. Kuhl[24], M. Kupper[23], G.D. La erty[15], H. Landsman[20], D. Lanske[13], D. Lellouch[23], J. Letts[o], L. Levinson[23], J. Lillich[9], S.L. Lloyd[12], F.K. Loebinger[15], J. Lu[26,b], A. Ludwig[3,t], J. Ludwig[9], W. Mader[3,t], S. Marcellini[2], A.J. Martin[12], T. Mashimo[22], P. Mattig[m], J. McKenna[26], R.A. McPherson[25], F. Meijers[7], W. Menges[24], F.S. Merritt[8], H. Mes[6,a], N. Meyer[24], A. Michelini[2], S. Mihara[22], G. Mikenberg[23], D.J. Miller[14], W. Mohr[9], T. Mori[22], A. Mutter[9], K. Nagai[12], I. Nakamura[22,v], H. Nanjo[22], H.A. Neal[32], S.W. O'Neale[1;], A. Oh[7], M.J. Oreglia[8], S. Orito[22;], C. Pahl[31], G. Pasztor[4,g], J.R. Pater[15], J.E. Pilcher[8], J. Pinfold[27], D.E. Plane[7], O. Pooth[13], M. Przybycien[7,n], A. Quadt[31], K. Rabbertz[7,r], C. Rembser[7], P. Renkel[23], J.M. Roney[25], A.M. Rossi[2], Y. Rozen[20], K. Runge[9], K. Sachs[6], T. Saeki[22], E.K.G. Sarkisyan[7,j], A.D. Schaile[30], O. Schaile[30], P. Schar -Hansen[7], J. Schieck[31], T. Schorner-Sadenius[7,z], M. Schroder[7], M. Schumacher[3], R. Seuster[13,f], T.G. Shears[7,h], B.C. Shen[4], P. Sherwood[14], A. Skuja[16], A.M. Smith[7], R. Sobie[25], S. Soldner-Rembold[15], F. Spano[8,x], A. Stahl[13], D. Strom[18], R. Strohmer[30], S. Tarem[20], M. Tasevsky[7,d], R. Teuscher[8], M.A. Thomson[5], E. Torrence[18], D. Toya[22], I. Trigger[7,w], Z. Trocsanyi[29,e], E. Tsur[21], M.F. Turner-Watson[1], I. Ueda[22], B. Ujvari[29,e], C.F. Vollmer[30], P. Vannerem[9], R. Vertesi[29,e], M. Verzocchi[16], H. Voss[7,q], J. Vossebeld[7,h], C.P. Ward[5], D.R. Ward[5], P.M. Watkins[1], A.T. Watson[1], N.K. Watson[1], P.S. Wells[7], T. Wengler[7], N. Wermes[3], G.W. Wilson[15,k], J.A. Wilson[1], G. Wolf[23], T.R. Wyatt[15], S. Yamashita[22], D. Zer-Zion[4], L. Zivkovic[20]

[1]School of Physics and Astronomy, University of Birmingham, Birmingham B15 2TT, UK

[2]Dipartimento di Fisica dell' Universita di Bologna and INFN, I-40126 Bologna, Italy

[3]Physikalisches Institut, Universitat Bonn, D-53115 Bonn, Germany

[4]Department of Physics, University of California, Riverside CA 92521, USA

[5]Cavendish Laboratory, Cambridge CB3 0HE, UK

[6]Ottawa-Carleton Institute for Physics, Department of Physics, Carleton University, Ottawa, Ontario K1S 5B6, Canada

[7]CERN, European Organisation for Nuclear Research, CH-1211 Geneva 23, Switzerland

[8]Enrico Fermi Institute and Department of Physics, University of Chicago, Chicago IL 60637,

USA
[9]Fakultat fur Physik, Albert-Ludwigs-Universitat Freiburg, D-79104 Freiburg, Germany
[10]Physikalisches Institut, Universitat Heidelberg, D-69120 Heidelberg, Germany
[11]Indiana University, Department of Physics, Bloomington IN 47405, USA
[12]Queen Mary and Westfield College, University of London, London E1 4NS, UK
[13]Technische Hochschule Aachen, III Physikalisches Institut, Sommerfeldstrasse 26-28, D-52056 Aachen, Germany
[14]University College London, London WC1E 6BT, UK
[15]School of Physics and Astronomy, Schuster Laboratory, The University of Manchester M13 9PL, UK
[16]Department of Physics, University of Maryland, College Park, MD 20742, USA
[17]Laboratoire de Physique Nucleaire, Universite de Montreal, Montreal, Quebec H3C 3J7, Canada
[18]University of Oregon, Department of Physics, Eugene OR 97403, USA
[19]Rutherford Appleton Laboratory, Chilton, Didcot, Oxfordshire OX11 0QX, UK
[20]Department of Physics, Technion-Israel Institute of Technology, Haifa 32000, Israel
[21]Department of Physics and Astronomy, Tel Aviv University, Tel Aviv 69978, Israel
[22]International Centre for Elementary Particle Physics and Department of Physics, University of Tokyo, Tokyo 113-0033, and Kobe University, Kobe 657-8501, Japan
[23]Particle Physics Department, Weizmann Institute of Science, Rehovot 76100, Israel
[24]Universitat Hamburg/DESY, Institut fur Experimentalphysik, Notkestrasse 85, D-22607 Hamburg, Germany
[25]University of Victoria, Department of Physics, P O Box 3055, Victoria BC V8W 3P6, Canada
[26]University of British Columbia, Department of Physics, Vancouver BC V6T 1Z1, Canada
[27]University of Alberta, Department of Physics, Edmonton AB T6G 2J1, Canada
[28]Research Institute for Particle and Nuclear Physics, H-1525 Budapest, P O Box 49, Hungary
[29]Institute of Nuclear Research, H-4001 Debrecen, P O Box 51, Hungary
[30]Ludwig-Maximilians-Universitat Munchen, Sektion Physik, Am Coulombwall 1, D-85748 Garching, Germany
[31]Max-Planck-Institute fur Physik, Fohringer Ring 6, D-80805 Munchen, Germany
[32]Yale University, Department of Physics, New Haven, CT 06520, USA

[a] and at TRIUMF, Vancouver, Canada V6T 2A3
[b] now at University of Alberta
[c] and Institute of Nuclear Research, Debrecen, Hungary
[d] now at Institute of Physics, Academy of Sciences of the Czech Republic 18221 Prague, Czech Republic
[e] and Department of Experimental Physics, University of Debrecen, Hungary
[f] and MPI Munchen
[g] and Research Institute for Particle and Nuclear Physics, Budapest, Hungary
[h] now at University of Liverpool, Dept of Physics, Liverpool L69 3BX, U.K.
[i] now at Dept. Physics, University of Illinois at Urbana-Champaign, U.S.A.
[j] and The University of Manchester, M13 9PL, United Kingdom
[k] now at University of Kansas, Dept of Physics and Astronomy, Lawrence, KS 66045, U.S.A.
[l] now at University of Toronto, Dept of Physics, Toronto, Canada
[m] current address Bergische Universitat, Wuppertal, Germany
[n] now at University of Mining and Metallurgy, Cracow, Poland

[o] now at University of California, San Diego, U.S.A.
[p] now at The University of Melbourne, Victoria, Australia
[q] now at IPHE Universite de Lausanne, CH-1015 Lausanne, Switzerland
[r] now at IEKP Universitat Karlsruhe, Germany
[s] now at University of Antwerpen, Physics Department, B-2610 Antwerpen, Belgium; supported by Interuniversity Attraction Poles Programme – Belgian Science Policy
[t] now at Technische Universitat, Dresden, Germany
[u] and High Energy Accelerator Research Organisation (KEK), Tsukuba, Ibaraki, Japan
[v] now at University of Pennsylvania, Philadelphia, Pennsylvania, USA
[w] now at TRIUMF, Vancouver, Canada
[x] now at Columbia University
[y] now at CERN
[z] now at DESY
Deceased

1 Introduction

The space-time evolution of a source emitting particles can be probed using intensity interferometry. Bose-Einstein correlations (BECs) in pairs of identical bosons have been studied at different centre-of-mass energies and for different initial states (e^+e^- [1], pp and $p\bar{p}$ [2], lepton-hadron [3], nucleus-nucleus collisions [4]). BECs manifest themselves as enhancements in the production of identical bosons which are close to one another in phase space. They can be analysed in terms of the correlation function

$$C(p_1,p_2) = \frac{\rho(p_1,p_2)}{\rho_0(p_1,p_2)} \tag{1}$$

where p_1 and p_2 are the 4-momenta of the two bosons, $\rho(p_1,p_2)$ is the density of the two identical bosons and $\rho_0(p_1,p_2)$ is the two-particle density in the absence of BECs (reference sample). From the experimental correlation function one can extract the dimension of the source element (frequently called correlation length or radius of the emitting source), i.e. the length of the region of homogeneity from which pions are emitted that have momenta similar enough to interfere and contribute to the correlation function.

At LEP Bose-Einstein correlations were analysed extensively in Z^0 hadronic events [5–11]. Two-pion correlations were studied as a function of the relative 4-momentum $q = \sqrt{-(p_1 - p_2)^2}$ of the pair: $C(p_1,p_2) = C(q)$. It was found that the radius of the emitting region, supposed spherical, is of the order of 1 fm and increases with the number of jets in the event [5]. No significant differences were observed in the source dimensions between the $\pi^\pm\pi^\pm$ and the $\pi^0\pi^0$ systems [6]; on the other hand, smaller radii were measured in $K^\pm K^\pm$ and K^0K^0 ($\overline{K^0K^0}$) pairs compared with pion pairs [7]. Genuine three-pion BECs were also observed [8]. Up to fifth-order genuine correlations of identically charged pions were obtained by OPAL [9], where BECs were shown to be an essential ingredient of the correlation scaling observed there, also for all-charged higher-order correlations. The hypothesis that the source is spherical was tested studying the correlations in terms of components of q: two- and three-dimensional analyses have shown that the pion emission region is elongated rather than spherical, with the longitudinal dimension, along the event thrust axis, larger than the transverse one [10, 11]. BECs were also studied in $e^+e^- \to W^+W^-$ events: no evidence of correlations between pions originating from different W bosons was found [12].

All the results listed above were obtained under the hypothesis that the momentum distribution of the emitted particles is homogeneous throughout the source elements, as would happen if the source is static. In the case of a dynamic, i.e. expanding, source, the dimension of the regions of homogeneity varies with the momentum of the emitted particles. The expansion leads to correlations between the space-time emission points and the particle 4-momenta (position-momentum correlations) which generate a dependence of the BEC radii on the pair momenta. In this case, the correlation function is expected to depend on the average 4-momentum of the pair $K = (p_1 + p_2)/2$ in addition to the relative 4-momentum q: $C(p_1,p_2) = C(q,K)$ [13], so that the measured radii correspond to regions of homogeneity in K, i.e. effective source elements of pairs with momentum K.

Published investigations of the source dynamics in e^+e^- collisions are available at energies lower than LEP's [1]. A dependence of the source radii on different components of the 4-vector K has been observed in more complex systems such as the emission region created after a high-energy collision between heavy nuclei. In particular, source radii have been found to decrease for increasing pair transverse momenta k_t (or, equivalently, transverse masses $m_t = \sqrt{k_t^2 + m^2}$) [4].

Hydrodynamical models for heavy ion collisions [14] explain this correlation in terms of an expansion of the source, due to collective flows generated by pressure gradients. A similar dependence of the size parameters on m_t was measured in pp collisions [15]. Longitudinal position-momentum correlations can be expected in e^+e^- annihilations as a consequence of string fragmentation [16]. Models based on different assumptions (the Heisenberg uncertainty principle [17], the generalized Bjorken-Gottfried hypothesis [18]) predict radii decreasing with the transverse mass also for sources created in e^+e^- collisions.

In this paper, which continues a series of OPAL studies on BECs [5, 10], a measurement of three-dimensional Bose-Einstein correlation functions is presented and the correlation functions are analyzed in order to measure their dependence on K and investigate potential dynamical features of the pion-emitting source created after an e^+e^- annihilation at a centre-of-mass energy of about 91 GeV.

2 Experimental procedure

A detailed description of the OPAL detector can be found in [19, 20]. In the present analysis, we have used the same data sample, about 4.3 million multihadronic events from Z^0 decays, and have applied the following selection cuts on tracks and events, identical to the ones described in [10]. First, the event thrust axis was computed, using tracks with a minimum of 20 hits in the jet chamber, a minimum transverse momentum of 150 MeV and a maximum momentum of 65 GeV. Clusters in the electromagnetic calorimeter are used if their energies exceed 100 MeV in the barrel or 200 MeV in the endcaps. Only events well contained in the detector were accepted, requiring $|\cos\theta_{thrust}| < 0.9$, where θ_{thrust} is the polar angle of the thrust axis with respect to the beam axis [1]. Then, a set of cuts, specific to BEC analyses, were applied. Tracks were required to have a maximum momentum of 40 GeV and to originate from the interaction vertex. Electron-positron pairs from photon conversions were rejected. Events were selected if they contained a minimum number of five tracks and if they were reasonably balanced in charge, i.e. requiring $|n^+_{ch} - n^-_{ch}|/(n^+_{ch} + n^-_{ch}) \leq 0.4$, where n^+_{ch} and n^-_{ch} are the number of positive and negative charge tracks, respectively. About 3.7 million events were left after all quality cuts. All charged particle tracks that passed the selections were used, the pion purity being approximately 90%. No corrections were applied for final state Coulomb interactions. All data and Monte Carlo distributions presented here are given at the detector level, i.e. not corrected for effects of detector acceptance and resolution.

The correlations were measured as functions of two different sets of variables, components of the pair 4-momentum difference q in two different frames.

The first set, $(Q_\ell, Q_{t_{side}}, Q_{t_{out}})$, was evaluated in the Longitudinally CoMoving System (LCMS) [21]. For each pion pair, the LCMS is the frame, moving along the thrust axis, in which the sum of the two particle momenta, $\vec{p} = (\vec{p}_1 + \vec{p}_2)$, lies in the plane perpendicular to the event thrust axis. The momentum difference of the pair, $\vec{Q} = (\vec{p}_1 - \vec{p}_2)$ is resolved into the moduli of the transverse component, $\vec{Q}_t$, and of the longitudinal component, $\vec{Q}_\ell$, where the longitudinal $(\hat{\ell})$ direction coincides with the thrust axis. $\vec{Q}_t$ may in turn be resolved into "out", $Q_{t_{out}}$, and "side", $Q_{t_{side}}$, components

$$\vec{Q}_t = Q_{t_{out}}\hat{o} + Q_{t_{side}}\hat{s} \tag{2}$$

[1] The coordinate system is defined so that z is the coordinate parallel to the e^+ and e^- beams, with positive direction along the e^- beam; r is the coordinate normal to the beam axis, ϕ is the azimuthal angle and θ is the polar angle with respect to $+z$.

where $\hat{o}$ and $\hat{s}$ are unit vectors in the plane perpendicular to the thrust direction, such that $\vec{p} = p\hat{o}$ defines the "out" direction and $\hat{s} = \hat{\tau} \times \hat{o}$ defines the "side" direction. It can be shown [22] that, in the LCMS, the components $Q_{t_{side}}$ and Q_{ℓ} reflect only the difference in emission space of the two pions, while $Q_{t_{out}}$ depends on the difference in emission time as well.

The second set, (q_t, q_ℓ, q_0), was evaluated in the event centre-of-mass (CMS) frame. For each event, two hemispheres are defined by the plane perpendicular to the thrust axis. Each pair is then associated to the hemisphere containing the vector sum of the three-momenta. The pair 4-momentum difference q is resolved into the energy difference $q_0 = (E_1 - E_2)$ and the 3-momentum difference $\vec{q} = (\vec{p}_1 - \vec{p}_2)$. The vector $\vec{q}$ is further decomposed into q_t and q_ℓ, the transverse and longitudinal components, respectively, with respect to the thrust axis. In each pair, index 1 corresponds to the particle with the highest energy, so that $q_0 \geq 0$. The longitudinal component, q_ℓ, may be either positive, in case the vector difference $\vec{q}$ lies in the pair hemisphere, or negative, in the opposite case. The transverse component, q_t, is positive definite.

The experimental three-dimensional correlation functions C are defined, in a small phase space volume around each triplet of Q_ℓ, $Q_{t_{side}}$ and $Q_{t_{out}}$ (or q_t, q_ℓ and q_0) values, as the number of like-charge pairs in that volume divided by the number of unlike-charge pairs:

$$C = \frac{N_{\pi^+\pi^+} + N_{\pi^-\pi^-}}{N_{\pi^+\pi^-}} = \frac{N_{like}}{N_{unlike}}. \tag{3}$$

In order to have adequate statistics in each bin, a bin size of 40 MeV was chosen in each component of q, which is larger than the estimated detector resolution of 25 MeV [5].

Long-range correlations are present in the correlation function C, due to phase space limitations and charge conservation constraints. In addition, the choice of unlike-sign pairs as the reference sample adds further distortions to the correlation function, due to pions from resonance decays. To reduce these effects, we introduced the (double) ratio C' of the correlation functions C in the data and in a sample of 7.2 million Jetset 7.4 [23] multihadronic Monte Carlo (MC) events, without BECs:

$$C' = \frac{C^{DATA}}{C^{MC}} = \frac{N^{DATA}_{like}/N^{DATA}_{unlike}}{N^{MC}_{like}/N^{MC}_{unlike}}. \tag{4}$$

The Monte Carlo samples are processed through a full simulation of the OPAL detector [24]. The simulation parameters of the generator were tuned in [25].

The dependence of the correlation functions $C'(q_t, q_\ell, q_0)$ and $C'(Q_\ell, Q_{t_{side}}, Q_{t_{out}})$ on the pair average 4-momentum K has been analyzed by selecting pions in different intervals of two components of K: the pair rapidity

$$|Y| = \frac{1}{2}\ln\left[\frac{(E_1+E_2)+(p_{\ell,1}+p_{\ell,2})}{(E_1+E_2)-(p_{\ell,1}+p_{\ell,2})}\right] \tag{5}$$

and the pair average transverse momentum with respect to the event thrust direction

$$k_t = \frac{1}{2}|(\vec{p}_{t,1} + \vec{p}_{t,2})|. \tag{6}$$

The differential $|Y|$ and k_t distributions, $\frac{dn}{d|Y|}$ and $\frac{dn}{dk_t}$, of the data are shown in Fig. 1. The same distributions for Jetset events are also presented in Fig. 1: the comparison shows a good agreement between data and Monte Carlo events.

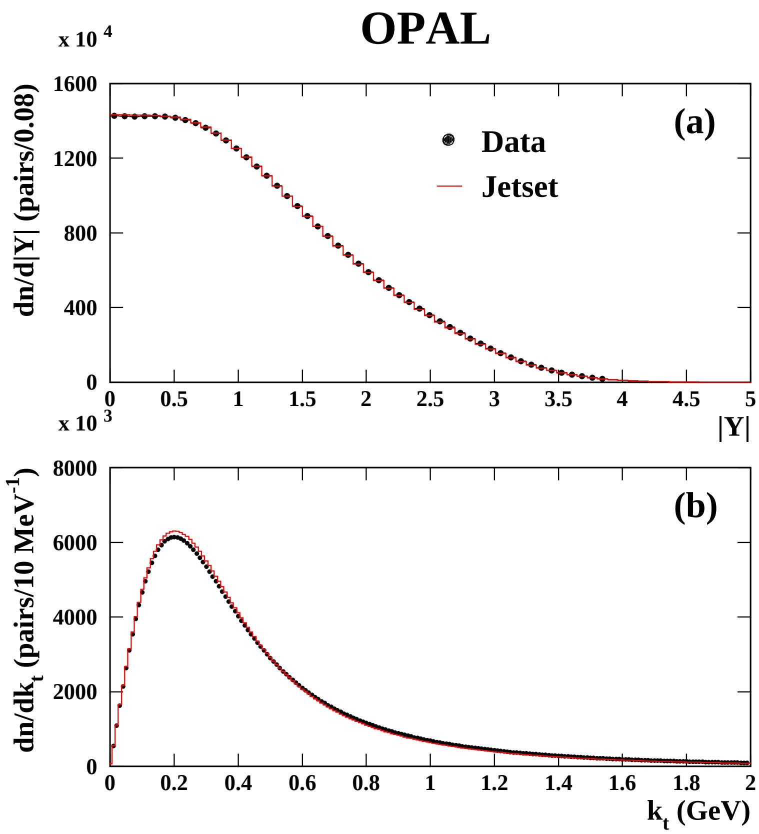

Figure 1: (a) Histogram of the differential distribution in the pair rapidity $|Y|$ and (b) in the pair mean transverse momentum k_t of the data (dots) and Jetset events (line). The number of pairs in the Monte Carlo sample has been normalized to the number of pairs in the data sample.

The dependence of C and C' on K has been studied in three bins of $|Y|$ ($0.0 \le |Y| < 0.8$, $0.8 \le |Y| < 1.6$, $1.6 \le |Y| < 2.4$) and five bins of k_t ($0.1 \le k_t < 0.2$ GeV, $0.2 \le k_t < 0.3$ GeV, $0.3 \le k_t < 0.4$ GeV, $0.4 \le k_t < 0.5$ GeV, $0.5 \le k_t < 0.6$ GeV). In this domain, a total of 47.3 million like-charge and 54.7 million unlike-charge pairs have been analysed.

3 The experimental correlation functions

Samples of two-dimensional projections of the correlation function $C(Q_\ell, Q_{t_{side}}, Q_{t_{out}})$ for a single bin of $|Y|$ and k_t are shown in Fig. 2 for the data and the MC Jetset events. For the example shown[2], the bin corresponding to pair rapidities and transverse momenta in the intervals $0.8 \le |Y| < 1.6$ and $0.3\ \text{GeV} \le k_t < 0.4$ GeV was chosen. Small (< 0.2 GeV) values of $Q_{t_{out}}$ and of Q_ℓ have been required in the $(Q_\ell, Q_{t_{side}})$ and in the $(Q_{t_{side}}, Q_{t_{out}})$ projections, respectively. Bose-Einstein correlation peaks are visible in the data at low $Q_\ell, Q_{t_{side}}, Q_{t_{out}}$ but they are not present in the Monte Carlo samples. The same two-dimensional projections for the correlation function $C'(Q_\ell, Q_{t_{side}}, Q_{t_{out}})$ are presented in Fig. 3(a) and (b). Also shown, in Fig. 3(c), (d) and (e), are the one-dimensional projections for low (< 0.2 GeV) values of the other two variables.

[2] Files of the three-dimensional correlation functions will be made available in the Durham HEP database.

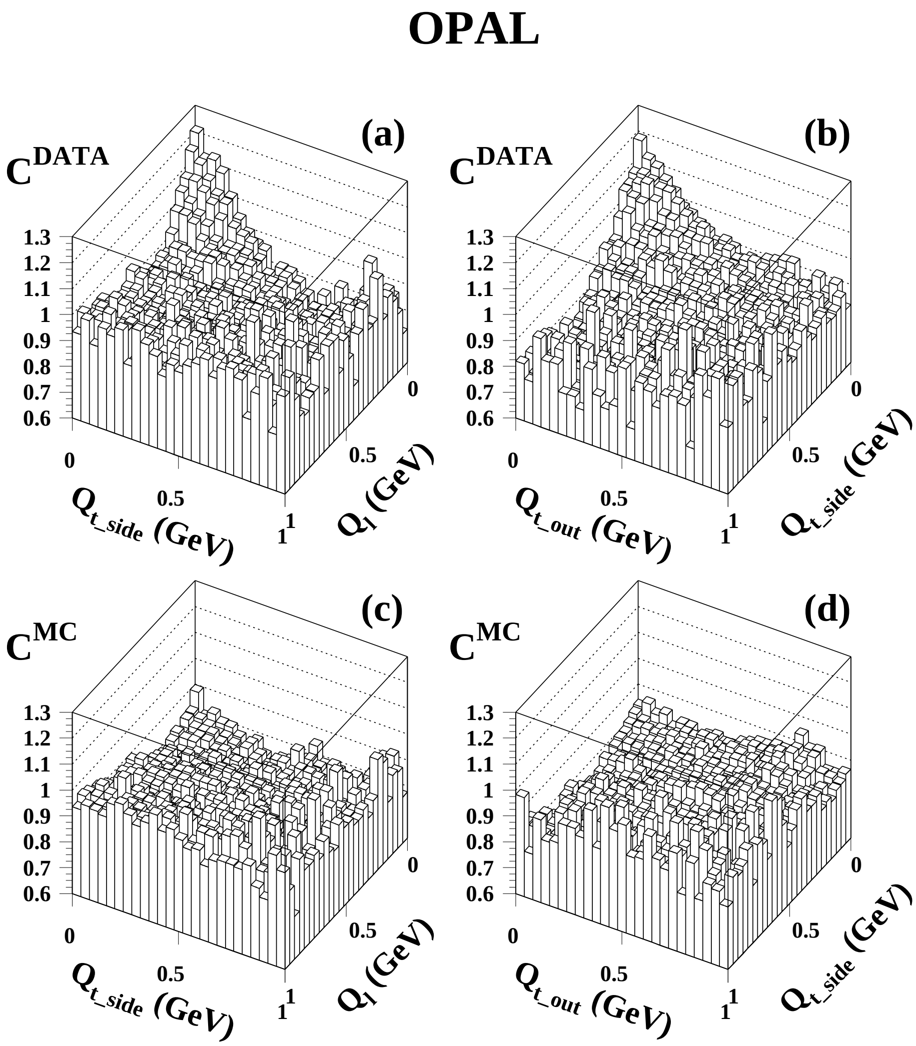

Figure 2: Two-dimensional projections of the correlation function $C(Q_\ell, Q_{t_{side}}, Q_{t_{out}})$ for $0.8 \leq |Y| < 1.6$ and $0.3\ \mathrm{GeV} \leq k_t < 0.4\ \mathrm{GeV}$ for the data ((a) and (b)) and for Jetset MC events ((c) and (d)). $Q_{t_{out}} < 0.2$ GeV in (a) and (c); $Q_\ell < 0.2$ GeV in (b) and (d).

The two-dimensional (q_ℓ, q_0) and the one-dimensional q_t projections of the correlation function $C(q_t, q_\ell, q_0)$ in the bin $0.8 \leq |Y| < 1.6$ and $0.3\ \mathrm{GeV} \leq k_t < 0.4\ \mathrm{GeV}$ are shown in Fig. 4, for data and Jetset events. Narrow cuts (< 0.2 GeV) on the other variables have been applied to make the projections. The combination $[(q_t^2 + q_\ell^2) - q_0^2]$ of the three variables is an invariant greater than zero. This condition and the bound on the pair rapidity constrain the correlation function to be different from zero only in a limited region of the (q_ℓ, q_0) plane, as can be seen in Fig. 4 (a) and (c). The (q_ℓ, q_0) and (q_ℓ, q_t) projections of the correlation function $C'(q_t, q_\ell, q_0)$ are shown in Fig. 5 together with the one-dimensional projections, for small (< 0.2 GeV) values of the other variables. BEC enhancements are clearly seen in both the q_t and q_ℓ projections, Fig. 5 (c) and (e). Fig. 5 (d), on the other hand, shows that the range available to the variable q_0 is quite restricted, and that no Bose-Einstein peak can be observed.

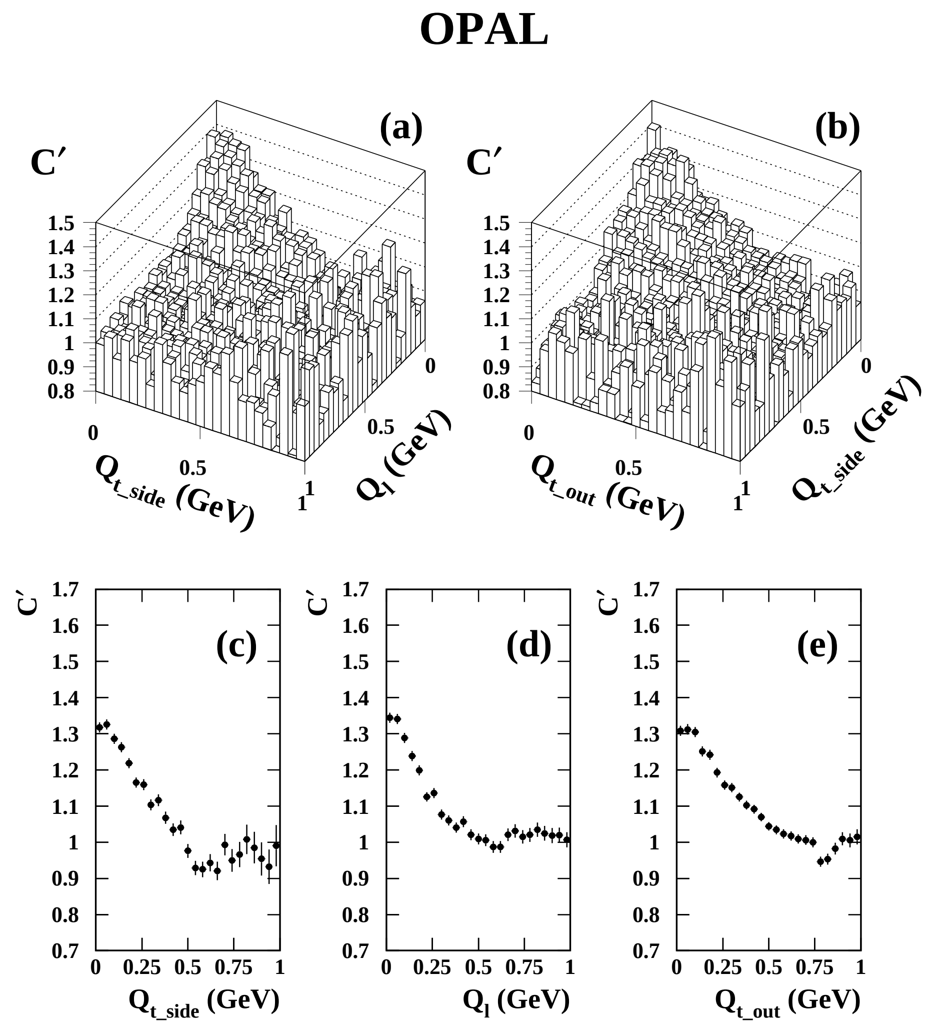

Figure 3: Two-dimensional ((a) and (b)) and one-dimensional ((c), (d) and (e)) projections of the correlation function $C'(Q_\ell, Q_{t_{side}}, Q_{t_{out}})$ for $0.8 \leq |Y| < 1.6$ and 0.3 GeV $\leq k_t < 0.4$ GeV. $Q_{t_{out}} < 0.2$ GeV in (a), $Q_\ell < 0.2$ GeV in (b). In (c), (d) and (e) the one-dimensional projections are obtained for low values (< 0.2 GeV) of the remaining two variables.

4 Parameterizations of the correlation functions

To extract the spatial and temporal extensions of the pion source from the experimental correlation functions, the Bertsch-Pratt (BP) [26]

$$C'(Q_\ell, Q_{t_{side}}, Q_{t_{out}})$$

$$= N\left(1 + \lambda e^{-(Q_\ell^2 R_{long}^2 + Q_{t_{side}}^2 R_{t_{side}}^2 + Q_{t_{out}}^2 R_{t_{out}}^2 + 2Q_\ell Q_{t_{out}} R_{long,t_{out}}^2)}\right) F(Q_\ell, Q_{t_{side}}, Q_{t_{out}}) \quad (7)$$

and the Yano-Koonin (YK) [27]

$$C'(q_t, q_\ell, q_0) = N\left(1 + \lambda e^{-(q_t^2 R_t^2 + \gamma^2 (q_\ell - v q_0)^2 R_\ell^2 + \gamma^2 (q_0 - v q_\ell)^2 R_0^2)}\right) F(q_t, q_\ell, q_0) \quad (8)$$

parameterizations were fitted to the measured correlation functions in all intervals of k_t and $|Y|$.

In both parameterizations, N is a normalization factor while λ measures the degree of incoherence of the pion sources, and is related to the fraction of pairs that actually interfere.

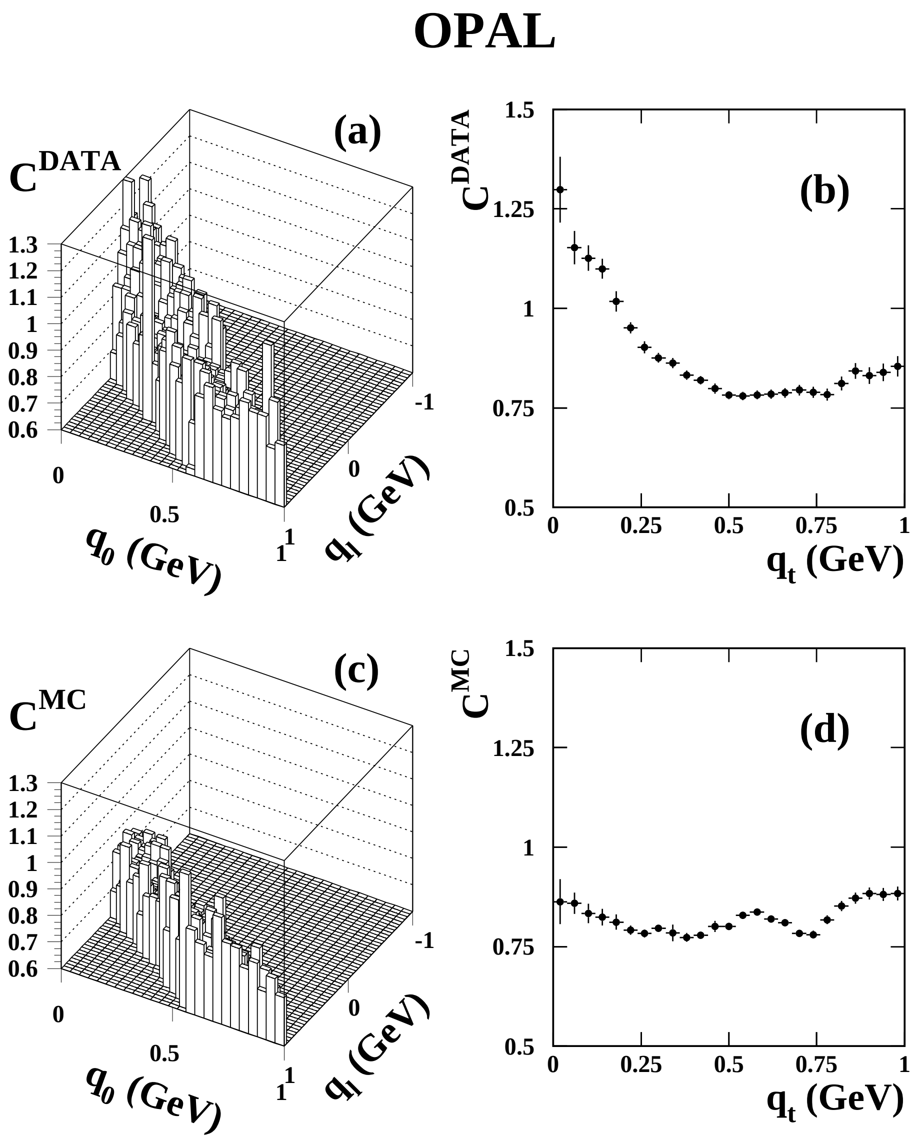

Figure 4: Two-dimensional (q_ℓ, q_0) and one-dimensional q_t projections of the correlation function $C(q_t, q_\ell, q_0)$ for data ((a) and (b)) and Jetset events ((c) and (d)). The correlation function was measured in the bin $0.8 \le |Y| < 1.6$ and 0.3 GeV $\le k_t < 0.4$ GeV. It was required $q_t < 0.2$ GeV in (a) and (c). In (b) and (d) the one-dimensional projections are obtained for low values (< 0.2 GeV) of the remaining two variables.

The two parameters N and λ, whose product determines the size of the BEC peak, are however significantly (anti)correlated: this limits the interpretation of λ and the comparison of its values between the two parameterizations.

The two functions $F(Q_\ell, Q_{t_{side}}, Q_{t_{out}}) = (1 + \delta_{long} Q_\ell + \delta_{t_{side}} Q_{t_{side}} + \delta_{t_{out}} Q_{t_{out}})$ and $F(q_t, q_\ell, q_0) = (1 + \epsilon_t q_t + \epsilon_\ell q_\ell + \epsilon_0 q_0)$, where δ_i and ϵ_i are free parameters, were introduced in Eq. (7) and (8) to take into account residual long-range two-particle correlations, due to energy and charge conservation.

The interpretation of the other free parameters in Eq (7), is the following:

- $R_{t_{side}}$ and R_{long} are the transverse and longitudinal source radii in the LCMS, i.e. the longitudinal rest frame of the pair;

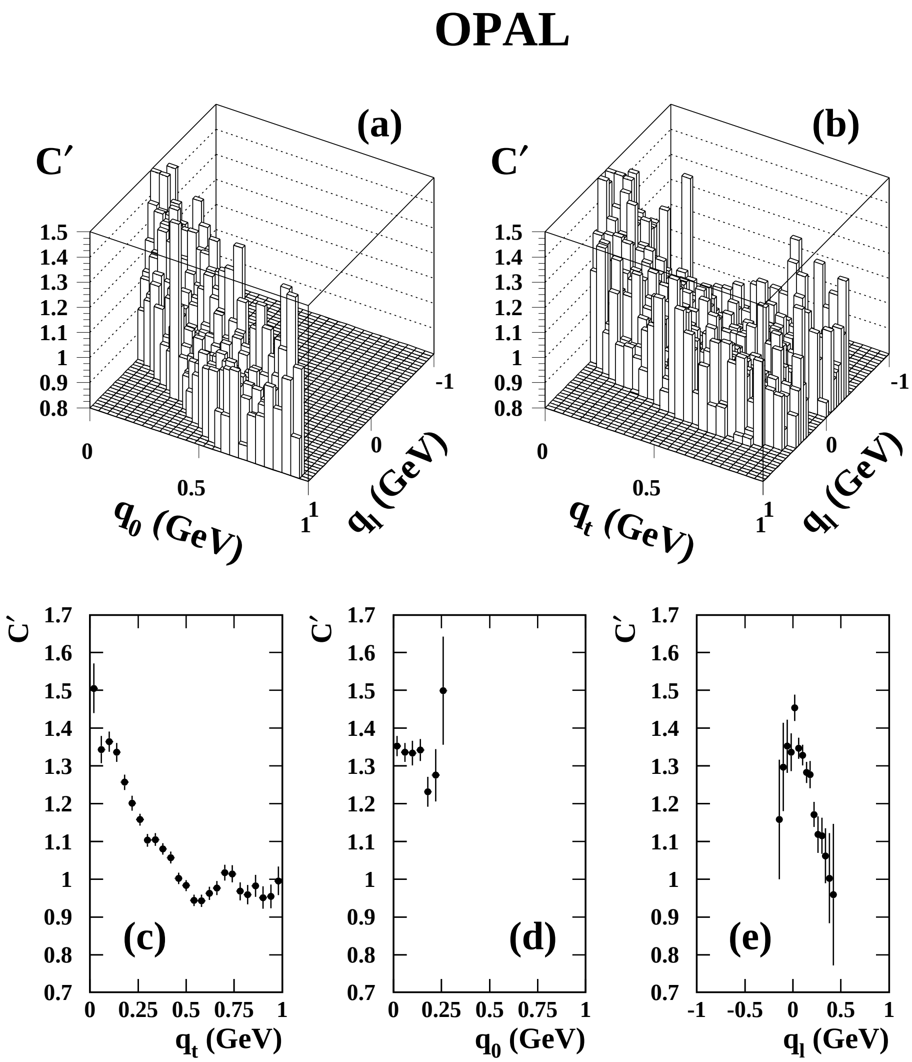

Figure 5: Two-dimensional projections of the correlation function $C'(q_t,q_\ell,q_0)$: (q_ℓ,q_0) for $q_t <$ 0.2 GeV in (a) and (q_ℓ,q_t) for $q_0 <$ 0.2 GeV in (b). One-dimensional projections ((c), (d) and (e)) of $C'(q_t,q_\ell,q_0)$, obtained for low values (< 0.2 GeV) of the remaining two variables. The correlation function has been measured in the bin $0.8 \le |Y| < 1.6$ and 0.3 GeV $\le k_t <$ 0.4 GeV.

- $R_{t_{out}}$ and the cross-term $R_{long,t_{out}}$ are a combination of both the spatial and temporal extentions of the source. Under certain assumptions [13], the difference $(R^2_{t_{out}} - R^2_{t_{side}})$ is proportional to the duration of the particle emission process, and $R_{long,t_{out}}$ to the source velocity with respect to the pair rest frame [22].

In the YK function Eq. (8), where $\gamma = 1/\sqrt{1-v^2}$, the free parameters are interpreted as follows:

- v is the longitudinal velocity, in units of c, of the source element in the CMS frame;

- R_0 measures the time interval, times c, during which particles are emitted, in the rest frame of the emitter (source element). Difficulties in achieving reliable results for the time parameter R^2_0 in YK fits have been reported in the literature [28], due to the limited phase-space available in $\gamma^2(q_0 - vq_\ell)^2$;

R_t and R_ℓ are the transverse and longitudinal radii, i.e. the regions of homogeneity of the source, in the rest frame of the emitter.

The parameters R_0, R_t and R_ℓ do not depend on the frame in which the correlation function has been measured, since they are evaluated in the rest frame of the source element.

The two parameterizations are not independent [13], so that a comparison between the BP and the YK fits represents an important test.

5 Results

Minimum χ^2 fits of the Bertsch-Pratt and the Yano-Koonin parameterizations to the experimental correlation functions were performed using the MINUIT [29] program. The error associated to each entry of the three-dimensional matrices C and C^0 was computed attributing a Poissonian uncertainty to the number of like and unlike charge pairs in the corresponding bin. The fit range allowed to each variable was set between 40 MeV and 1 GeV. The region below 40 MeV was excluded to avoid problems of detector resolution and poorly reconstructed or split tracks which mimic two like charged particle tracks with very low q. In Sections 5.1 and 5.2 the results of the fits are presented. Sources of systematic uncertainties on the fit parameters are discussed in Section 5.3. Section 5.4 is devoted to a comparison between the BP and the YK parameterizations.

5.1 Bertsch-Pratt fits

The best-fit parameters of the BP function, Eq. (7), are listed in Table 1, and their dependence on $|Y|$ and k_t is shown in Fig. 6. Errors in Fig. 6 include both statistical standard deviations as given by the fit program [3] and systematic uncertainties (discussed in Section 5.3), added in quadrature. One notes that there is only a minor dependence on the rapidity, but some parameters depend on k_t. In more detail:

- λ varies between 0.25 and 0.4. The coefficient of correlation between the parameters λ and N is about -0.35, almost independent of k_t;
- $R^2_{t_{side}}$, $R^2_{t_{out}}$ and, less markedly, R^2_{long} decrease with increasing k_t. The presence of correlations between the particle production points and their momenta is an indication that the pion source is not static, but rather expands during the particle emission process. R^2_{long} is larger than the corresponding transverse parameter $R^2_{t_{side}}$, in agreement with a pion source which is elongated in the direction of the event thrust axis [10];
- the cross-term parameter $R^2_{long,t_{out}}$ is compatible with zero, apart from a few bins at the highest rapidity interval. This result may be explained [13] assuming that the source velocity, measured with respect to the rest frame of the pion pair, is close to zero;
- the difference between the "out" and "side" transverse parameters, $(R^2_{t_{out}} - R^2_{t_{side}})$ for $|Y| < 1.6$ is positive at low k_t, then it decreases and becomes negative for $k_t \geq 0.3$ GeV. In the highest rapidity interval, $1.6 \leq |Y| < 2.4$, $(R^2_{t_{out}} - R^2_{t_{side}})$ is compatible with zero, for all k_t. As a consequence, it is not possible to estimate the particle emission time from $(R^2_{t_{out}} - R^2_{t_{side}})$;

[3] The HESSE algorithm in MINUIT calculates the error matrix inverting the matrix of the second derivatives of the fit function with respect to the fit parameters.

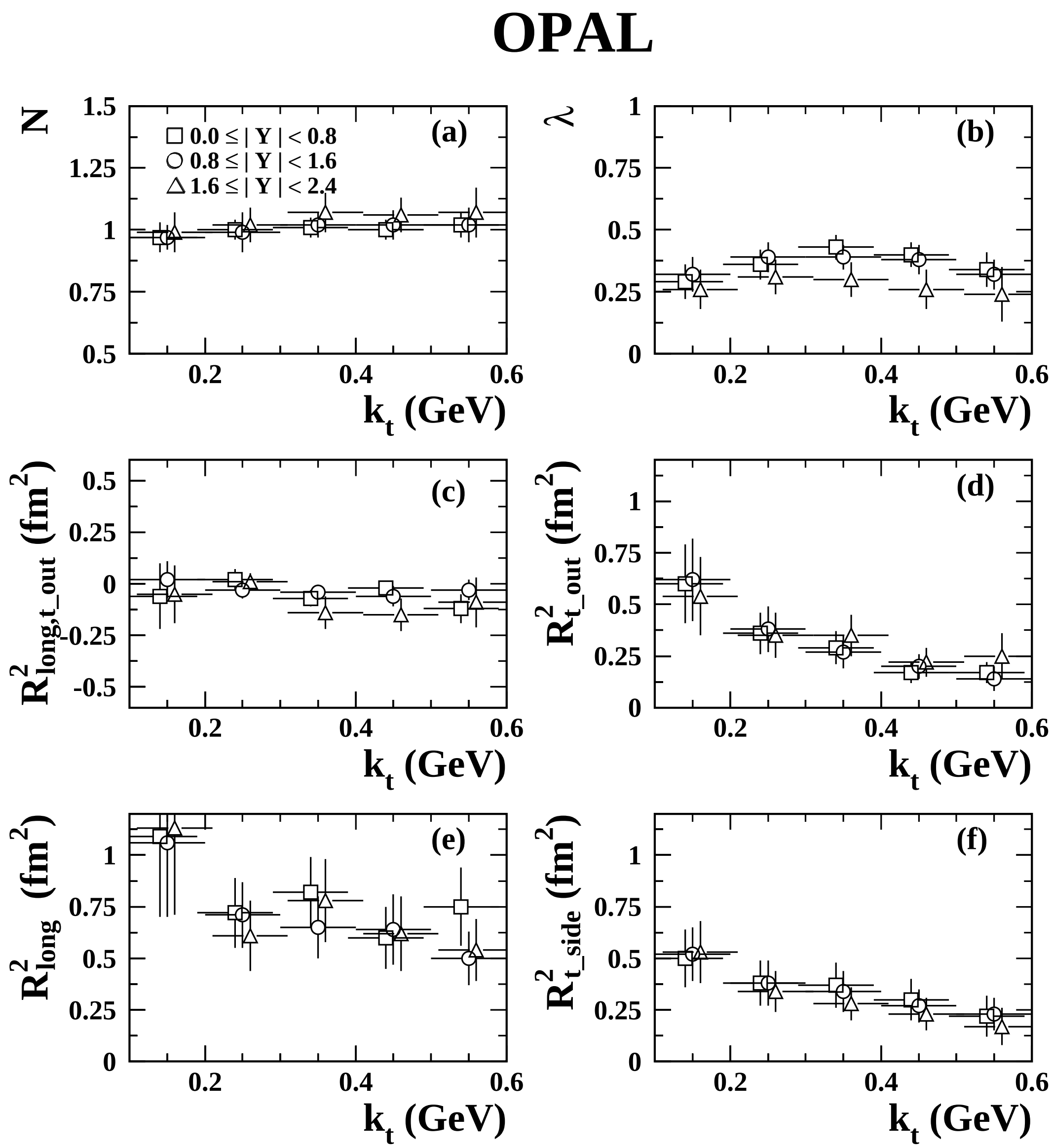

Figure 6: Best- t parameters of the Bertsch-Pratt parameterization, Eq. (7), to the correlation function $C^0(Q_\ell, Q_{t_{side}}, Q_{t_{out}})$, as a function of k_t, for di erent intervals of rapidity $|Y|$. The correlation functions were measured in the LCMS frame. Horizontal bars represent bin widths and vertical bars include both statistical and systematic errors. (a) the normalization factor N; (b) the incoherence parameter λ; (c) the cross term $R^2_{long,t_{out}}$; (d) the parameter $R^2_{t_{out}}$; (e) the squared longitudinal correlation length R^2_{long} and (f) the squared transverse correlation length $R^2_{t_{side}}$.

the parameters ϵ_i are not negligible: the function $F(Q_\ell, Q_{t_{side}}, Q_{t_{out}})$ typically di ers from unity for at most 15% to 20% at $Q_i \simeq 1$ GeV.

5.2 Yano-Koonin ts

Table 2 and Fig. 7 show the parameters of the YK ts, Eq. (8), in di erent $|Y|$ and k_t intervals. Error bars in Fig. 7 include both statistical and systematic uncertainties, added in quadrature. It can be seen that:

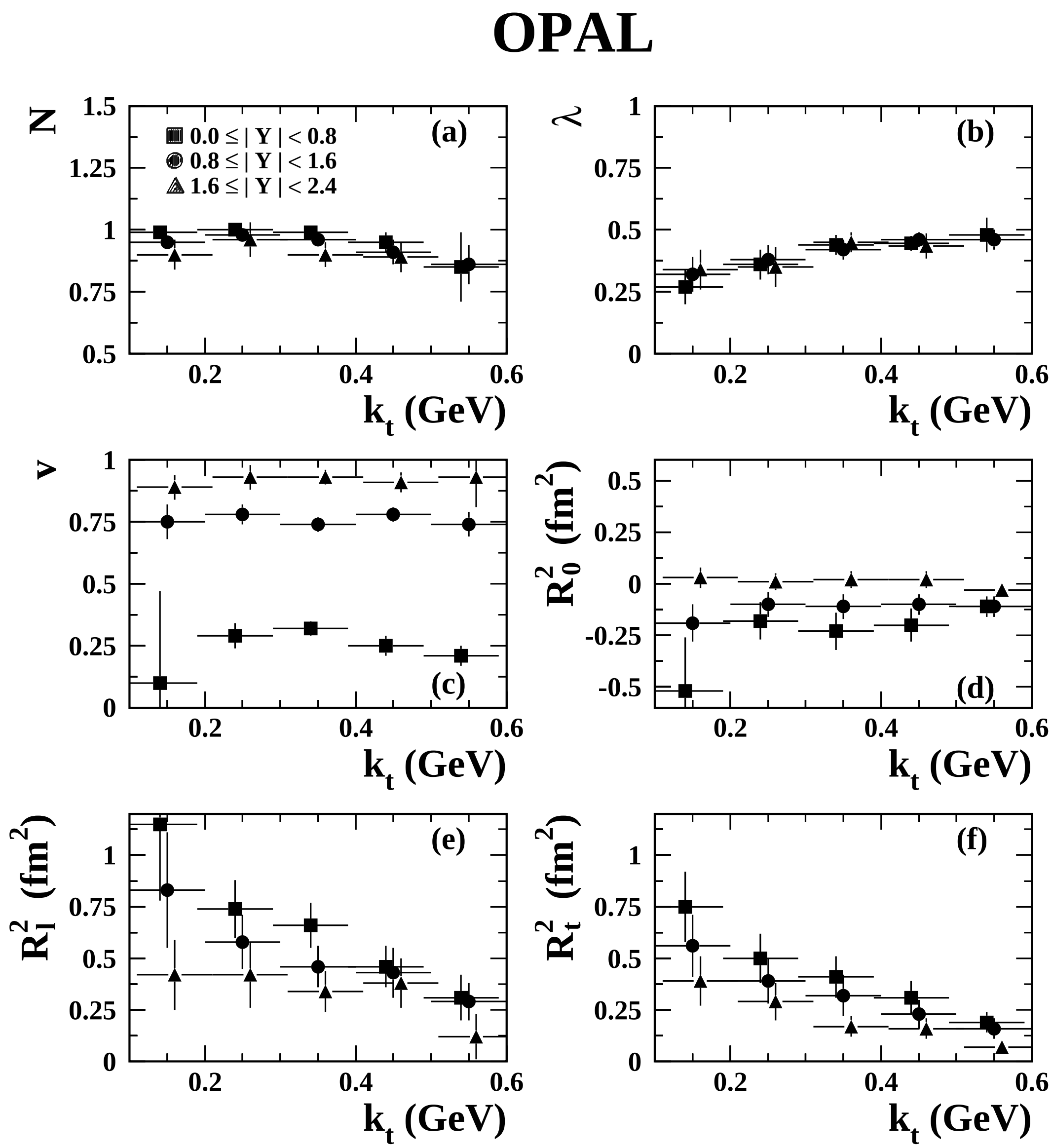

Figure 7: Best-fit parameters of the Yano-Koonin parameterization, Eq. (8), to the correlation function $C'(q_t, q_\ell, q_0)$, as a function of k_t, for different intervals of rapidity $|Y|$. The correlation functions were measured in the event centre-of-mass frame. Horizontal bars represent bin widths and vertical bars include both statistical and systematic errors. (a) the normalization factor N; (b) the parameter λ; (c) the source velocity v; (d) the time parameter R_0^2; (e) the squared longitudinal correlation length R_ℓ^2 and (f) the squared transverse correlation length R_t^2.

- the parameter λ is almost independent of rapidity and increases with k_t, reaching values of about 0.5 for the largest k_t values. It is however significantly anticorrelated with the parameter N, the correlation coefficient increasing in absolute value from about -0.50 at low k_t up to -0.80 for $k_t > 0.4$ GeV;

- both R_t^2 and R_ℓ^2 decrease with increasing k_t and $|Y|$. The longitudinal radii are larger than the transverse radii. This agrees with an expanding, longitudinally elongated source;

- R_0^2 is compatible with zero at high rapidities, and assumes negative values for $|Y| < 1.6$. This excludes an interpretation of R_0/c in terms of the time duration of the particle emission process;

- those of the parameters $_i$ which are not negligible, contribute typically 10% to 15% to the function $F(q_t;q_\ell;q_0)$ at large q_i;
- the source velocity v does not depend on k_t, but it is strongly correlated with the pair rapidity.

The dependence of v on $|Y|$ can also be presented [30,4] in terms of a plot a la GIBS, i.e. the Yano-Koonin rapidity

$$Y_{YK} = \frac{1}{2}\ln\left(\frac{1+v}{1-v}\right) \tag{9}$$

as a function of the pair rapidity $|Y|$. Y_{YK} measures the rapidity of the source element with respect to the centre-of-mass frame: a non-expanding source would therefore correspond to $Y_{YK} \approx 0$ for any $|Y|$. On the other hand, for a boost-invariant source [4], the strict correlation $Y_{YK} = |Y|$ is expected [13,27], since only the source elements which move with velocities close to the velocity of the observed particle pair contribute to the correlation function. In Fig. 8 the Yano-Koonin rapidity Y_{YK} is shown as a function of the pair rapidity. Since in a given $|Y|$ interval the parameter v is almost independent of k_t, see Fig. 7(c), each Y_{YK} is computed, according to Eq. (9), using the average value of v over all k_t in that $|Y|$ bin. Each $|Y|$ has been computed as the weighted average of the corresponding bin, rather than the centre of the bin. A clear positive correlation between Y_{YK} and $|Y|$ is observed, even if $Y_{YK} < |Y|$ at the largest pair rapidities. This is in agreement with a pion source which is emitting particles in a nearly boost-invariant way.

To try to understand the YK fit results of the parameter R_0^2, it is useful to analyse the two-dimensional projection $(q_\ell;q_0)$ of the correlation function $C^0(q_t;q_\ell;q_0)$ after the longitudinal boost to the rest frame of the source element. We then introduce $q_\ell^{boost} = \gamma(q_\ell - vq_0)$ and $q_0^{boost} = \gamma(q_0 - vq_\ell)$, where the best-fit parameter v is used to boost the variables. In Fig. 9(a) the two-dimensional $(|q_\ell^{boost}|,|q_0^{boost}|)$ projection of C^0 is presented. The phase space available to $|q_0^{boost}|$ is limited, when q_t approaches 0, and the one-dimensional $|q_0^{boost}|$ projection (Fig. 9(b)) is approximately flat: it is not possible to distinguish any peak due to Bose-Einstein correlations and, for most rapidity and k_t intervals, the fitted R_0^2 have negative values. In Fig. 9(b), the solid line shows the one-dimensional $|q_0^{boost}|$ projection ($|q_\ell^{boost}| < 0.2$ GeV, $q_t < 0.2$ GeV) of the YK fit, Eq. (8); the line is an increasing function of q_0^{boost}, because of the negative value of R_0^2. Similar limitations in the temporal acceptance have been reported in the literature [28]. On the other hand, the $|q_\ell^{boost}|$ projection for $|q_0^{boost}| < 0.2$ GeV and $q_t < 0.2$ GeV, Fig. 9(c), shows a clear BEC peak at small $|q_\ell^{boost}|$, reproduced by the one dimensional $|q_\ell^{boost}|$ projection of the best-fit YK function (solid line).

5.3 Systematic effects

The systematic uncertainties of the fit parameters and the stability of the results concerning the dependence of the transverse and longitudinal radii on k_t was studied by considering a number of changes with respect to the reference analysis. The following changes were taken into account:

[4] A source expands boost-invariantly in the longitudinal direction if the velocity of each element is given by $v = z/t$, where t and z are, respectively, the time elapsed since the collision and the longitudinal coordinate of the element, in the centre-of-mass frame. In that case, particle emission happens at constant proper times $\sqrt{t^2 - z^2}$.

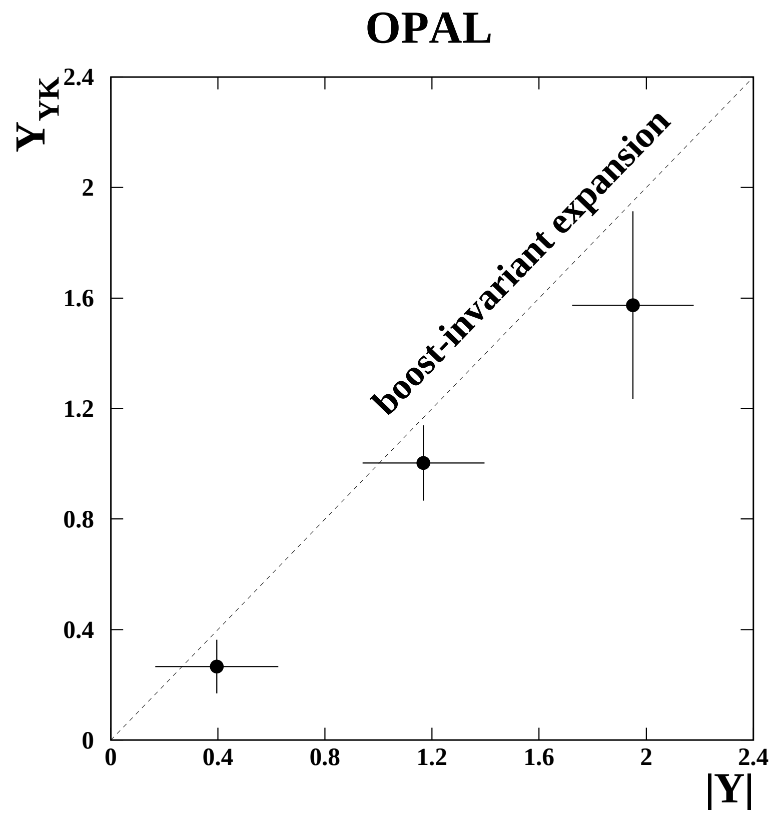

Figure 8: The Yano-Koonin rapidity Y_{YK} plotted versus the pion pair rapidity $|Y|$. Each $|Y|$ was computed as the weighted average of the corresponding bin. Y_{YK} values were computed by means of Eq. (9), using the average value of v over all k_t in that $|Y|$ bin. Horizontal bars are r.m.s. deviations from the average. Vertical bars include both statistical and systematic errors. Also shown is the line $Y_{YK} = |Y|$, corresponding to a source which expands boost-invariantly.

- A correction was applied to the correlation functions, based on the Gamow factors [31], in order to take into account final-state Coulomb interactions between charged pions.

- The analysis was repeated with more stringent cuts in the selection: a maximum momentum of 30 GeV instead of 40 GeV and a charge unbalance smaller than 0.25 per event instead of 0.4.

- The fits were repeated changing the upper bound of the fit range from 1 GeV to 0.8 GeV.

In the cases listed above, we found negligible differences in the parameters with respect to the reference analysis. The systematic effect on the correlation function C', due to the Monte Carlo modelling, was assumed negligible.

- The correlation functions were measured in bins of 60 MeV, instead of 40 MeV, to test the stability of the fits. Bin widths larger than 60 MeV would prevent a correct reconstruction of the BEC peak, which is about 300 – 400 MeV wide.

- Possible non-Gaussian shapes of the correlation functions at low q were tested replacing the Gaussian functions in the BP and YK parameterizations with first order Edgeworth expansions [32] of the Gaussian. The χ^2/DoF of the two fits were found to be comparable.

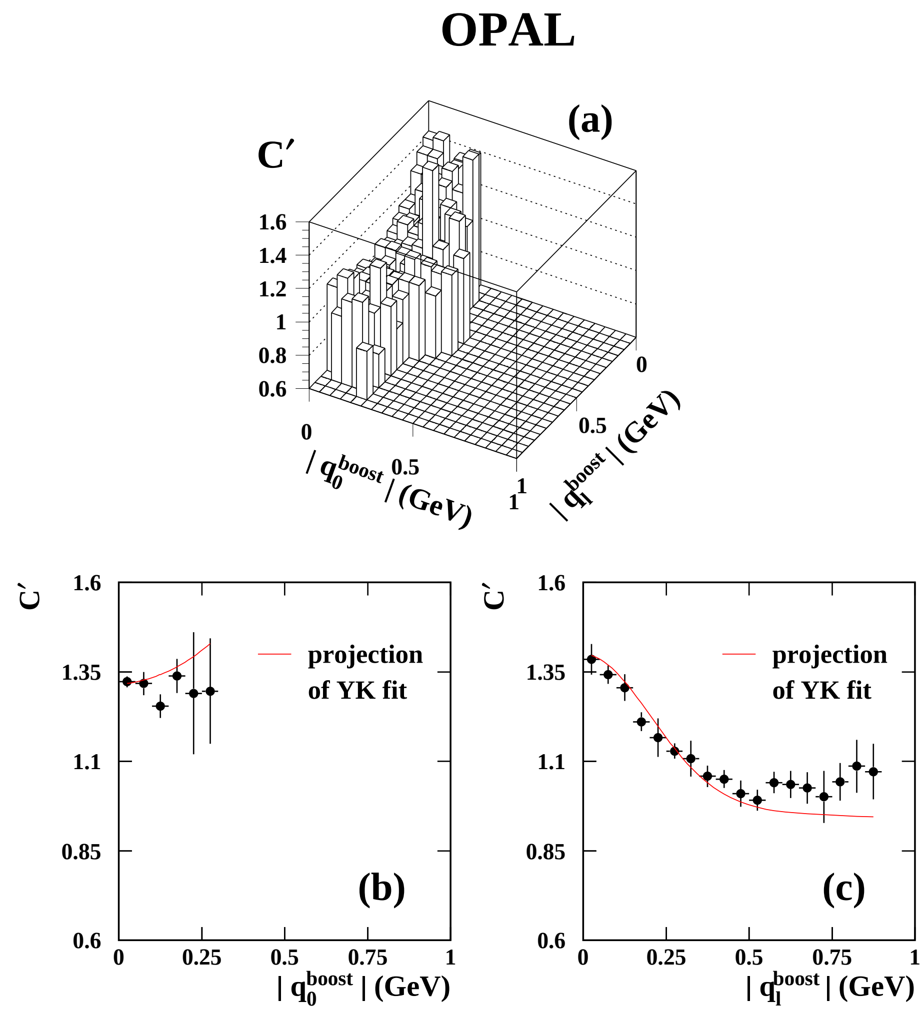

Figure 9: (a) The two-dimensional projection ($|q_l^{boost}|, |q_0^{boost}|$), after the longitudinal boost to the source element rest frame, measured for pion pairs in the rapidity interval $0.8 \leq |Y| < 1.6$ and with mean transverse momenta in the range 0.3 GeV $\leq k_t < 0.4$ GeV. The projection was made requiring $q_t < 0.2$ GeV.
(b) The one-dimensional projection in $|q_0^{boost}|$ ($|q_l^{boost}| < 0.2$ GeV). The curve is the one-dimensional projection of the Yano-Koonin three-dimensional best-fit function.
(c) The one-dimensional projection in $|q_l^{boost}|$ ($|q_0^{boost}| < 0.2$ GeV). The curve is the one-dimensional projection of the Yano-Koonin three-dimensional best-fit function.

Systematic errors on the fit parameters have been computed adding in quadrature the deviations from the standard fit; they are reported in Tables 1 and 2.

Assuming simple linear dependences of the squared BP and YK longitudinal and transverse radii on k_t, we measured the slopes, dR_i^2/dk_t, by minimum χ^2 fits. Fits were performed on the radii of the reference analysis, with statistical errors only. The systematic errors on the slopes were then estimated comparing the slopes from the reference analysis with the slopes from the systematic checks listed above. Table 3 shows the best-fit slopes with errors. In all cases a decrease of the radii with increasing k_t is favoured even if, in one rapidity interval, the longitudinal BP radius is compatible with independence on k_t.

To investigate further the decrease of the radii on k_t, the YK and BP functions were fitted to the correlation function C, Eq. (1). Larger (about 30%) squared transverse and longitudinal radii with respect to the correlation function C' are obtained in this case. However, the slopes of the linear dependences of the squared radii on k_t are the same, within uncertainties, for C and C'. A comparison of the YK best-fit parameters from minimizing χ^2 values and from maximizing a likelihood function [33] has been done for the correlation function C. The differences between the parameters fitted with the two techniques were negligible.

One more check was done on the YK transverse radius R_t: we computed the one-dimensional projection $C'(q_t;0;0)$ of the three-dimensional correlation function $C'(q_t;q_\parallel;q_0)$, by requiring $q_\parallel$ and $q_0 \leq 0.08$ GeV, and we fitted the function

$$C'(q_t) = N\,(1 + \lambda\, e^{-q_t^2 R_t^2}) \tag{10}$$

to the projection. We first checked that the best-fit R_t^2 is compatible, within errors, to the one we obtain if the right-hand side of Eq. (10) is multiplied by a "long-range" factor $(1 + \delta_t q_t)$. Based on the same one-dimensional projection $C'(q_t;0;0)$, we also measured the transverse correlation length in a λ_t-independent way [34], introducing the parameter $\tilde{R}_t$

$$\tilde{R}_t = \frac{1}{\sqrt{2\langle q_t^2\rangle}} \quad \text{where} \quad \langle q_t^2\rangle = \frac{\int q_t^2\,[C'(q_t;0;0) - 1]\,dq_t}{\int [C'(q_t;0;0) - 1]\,dq_t} \tag{11}$$

i.e. the inverse variance of the correlation function for small q_t values [5]. We found that $\tilde{R}_t$, computed using Eq. (11), agrees with the best-fit R_t from Eq. (10); the slope of the linear decrease is about 20% smaller than the one measured with three-dimensional YK fits, Eq. (8).

The standard analysis was also repeated for a subsample of events classified as two-jets by the Durham jet-finding algorithm [35]. The subsample was defined by setting the resolution parameter at $y_{cut} = 0.04$. The dependences of the best-fit parameters on $|Y|$ and k_t are similar to those found for the inclusive sample of events. In particular, the longitudinal and the transverse radii decrease with increasing k_t. However, the radii measured in the case of two-jet events are smaller, by about 10%, than in the inclusive sample [5]. An increase of the "jettyness" of the two-jet subsample, obtained using a smaller y_{cut} ($y_{cut} = 0.02$) in the jet-finding algorithm, does not change significantly the behaviour of the parameters.

5.4 Comparison between BP and YK fits

The following relations should hold between the correlation lengths of the BP and YK functions measured in the LCMS and CMS frames, respectively [13]:

$$
\begin{aligned}
R^2_{t_{side}} &= R^2_t & (12)\\
R^2_{long} &= \gamma^2_{LCMS}\,(R^2_\parallel + \beta^2_{LCMS} R^2_0) & (13)\\
(R^2_{t_{out}} - R^2_{t_{side}}) &= \beta^2_t\,\gamma^2_{LCMS}\,(R^2_0 + \beta^2_{LCMS} R^2_\parallel): & (14)
\end{aligned}
$$

In Eq. (13) and (14) β_{LCMS} is the velocity of the source element measured in the LCMS, i.e. with respect to the pair longitudinal rest frame; $\gamma_{LCMS} = 1/\sqrt{1 - \beta^2_{LCMS}}$. In Eq. (14) $\beta^2_t = \left\langle \frac{2k_t}{E_1 + E_2} \right\rangle^2$, where the brackets stand for the average over all pion pairs in the given $|Y|$ and k_t range. For a boost-invariant source, $\beta_{LCMS} = 0$ and Eqs. (13) and (14) reduce to:

$$
\begin{aligned}
R^2_{long} &= R^2_\parallel & (15)\\
(R^2_{t_{out}} - R^2_{t_{side}}) &= \beta^2_t R^2_0: & (16)
\end{aligned}
$$

[5] In the actual estimate of $\langle q_t^2\rangle$ we have computed $\frac{\sum q_t^2\,[C'(q_t;0;0) - N]}{\sum [C'(q_t;0;0) - N]}$, where N is the normalization parameter of the fit Eq. (10) and each q_t has been taken as the central value of the corresponding 40 MeV bin.

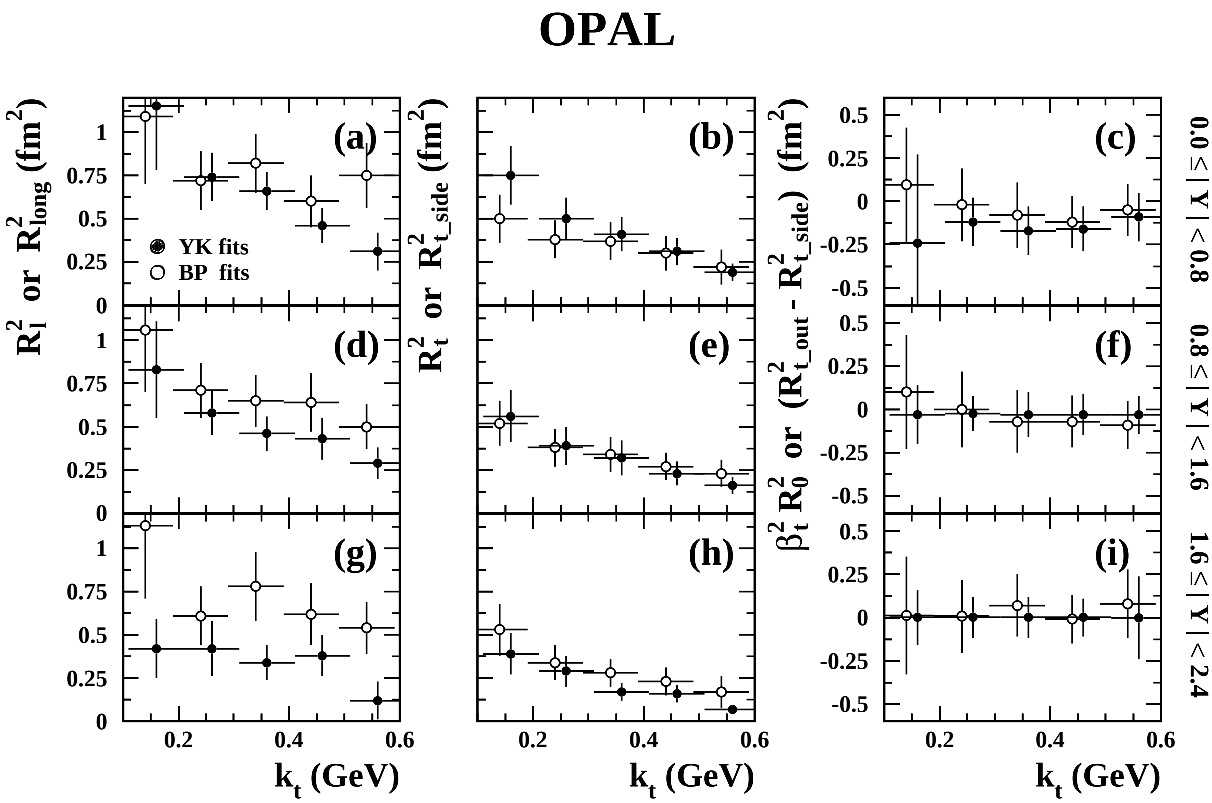

Figure 10: (a) (d) (g) The best-fit longitudinal radius R^2_{long} of the Bertsch-Pratt parameterization (open dots) compared with the Yano-Koonin longitudinal radius $R^2_{\parallel}$ (full dots). (b) (e) (h) The BP transverse correlation length $R^2_{t_{side}}$ (open dots) compared with the YK transverse correlation length R^2_t (full dots). (c) (f) (i) The difference of the BP transverse radii $(R^2_{t_{out}} - R^2_{t_{side}})$ (open dots) compared with the YK time parameter R^2_0 times β^2_t (full dots). Errors on the parameters include both statistical and systematic uncertainties, added in quadrature.

In Fig. 10 the best-fit BP parameters R^2_{long}, $R^2_{t_{side}}$ and $(R^2_{t_{out}} - R^2_{t_{side}})$ are compared with the YK parameters $R^2_{\parallel}$, R^2_t and $\beta^2_t R^2_0$.

The longitudinal parameter R^2_{long} is systematically larger than $R^2_{\parallel}$ in all the rapidity intervals analyzed (Fig. 10(a), (d) and (g)). According to Eq. (13), $R^2_{long} > R^2_{\parallel}$ corresponds to β_{LCMS} greater than zero, in agreement with a pion source whose expansion is not exactly boost-invariant.

The equality of the transverse parameters $R^2_{t_{side}}$ and R^2_t, Eq. (12), is confirmed within errors, with possible deviations at low k_t (Fig. 10(b), (e) and (h)).

The negative values of R^2_0 and $(R^2_{t_{out}} - R^2_{t_{side}})$ appearing in the two first rapidity intervals (Fig. 10(c), (f) and (i)) prevent an interpretation in terms of the time duration of the particle emission process. Negative values of R^2_0 have been suggested [36] as possible indicators for opacity of the source, i.e. surface dominated emission. A dependence of $(R^2_{t_{out}} - R^2_{t_{side}})$ on k_t similar to the one shown in Fig. 10(c) and (f) has been reported in heavy-ion collision experiments [37].

6 Conclusions

An analysis of Bose-Einstein correlations in e^+e^- annihilation events at the Z^0 peak performed in bins of the average 4-momentum of the pair, K, has been presented for the first time. Based on this, dynamic features of the pion emitting source were investigated. Previous BEC analyses, not differential in K, were not sensitive to these features.

Using the Yano-Koonin and the Bertsch-Pratt formalisms, the correlation functions were studied in intervals of two components of K: the pion pair rapidity $|Y|$ and the mean transverse momentum k_t. We found that the transverse and longitudinal radii of the pion sources decrease for increasing k_t, indicating the presence of correlations between the particle production points and their momenta. The Yano-Koonin rapidity scales approximately with the pair rapidity, in agreement with a nearly boost-invariant expansion of the source of pions. Limitations in the available phase space did not allow measurement of the duration of the particle emission process.

Similar results have been observed in more complex systems, such as the pion sources created in pp and heavy-ion collisions, which are now complemented with such measurements in the simpler hadronic system formed in e^+e^- annihilations.

Acknowledgements

We particularly wish to thank the SL Division for the efficient operation of the LEP accelerator at all energies and for their close cooperation with our experimental group. In addition to the support staff at our own institutions we are pleased to acknowledge the
Department of Energy, USA,
National Science Foundation, USA,
Particle Physics and Astronomy Research Council, UK,
Natural Sciences and Engineering Research Council, Canada,
Israel Science Foundation, administered by the Israel Academy of Science and Humanities,
Benoziyo Center for High Energy Physics,
Japanese Ministry of Education, Culture, Sports, Science and Technology (MEXT) and a grant under the MEXT International Science Research Program,
Japanese Society for the Promotion of Science (JSPS),
German Israeli Bi-national Science Foundation (GIF),
Bundesministerium für Bildung und Forschung, Germany,
National Research Council of Canada,
Hungarian Foundation for Scientific Research, OTKA T-038240, and T-042864,
The NWO/NATO Fund for Scientific Research, the Netherlands.

References

[1] TASSO Coll., D. Althoff et al., Z. Phys. C 30 (1986) 355;
AMY Coll., S.K. Choi et al., Phys. Lett. B 355 (1995) 406.

[2] ABCDHW Coll., A. Breakstone et al., Phys. Lett. B 162 (1985) 400;
UA1 Coll., C. Albajar et al., Phys. Lett. B 226 (1989) 410.

[3] WA25 Coll., D. Allasia et al., Z. Phys. C 37 (1988) 527;
H1 Coll., C. Adloff et al., Z. Phys. C 75 (1997) 437;
ZEUS Coll., S. Chekanov et al., Phys. Lett. B 583 (2004) 231.

[4] E877 Coll., J. Barrette et al., Nucl. Phys. A 610 (1996) 227c;
NA49 Coll., H. Appelshauser et al., Eur. Phys. J. C 2 (1998) 661;
WA97 Coll., F. Antinori et al., J. Phys. G 27 (2001) 2325;
PHOBOS Coll., B.B. Back et al., Phys. Rev. C 73 (2006) 031901.

[5] OPAL Coll., P.D. Acton et al., Phys. Lett. B 267 (1991) 143;
OPAL Coll., G. Alexander et al., Z. Phys. C 72 (1996) 389.

[6] L3 Coll., P. Achard et al., Phys. Lett. B 524 (2002) 55;
OPAL Coll., G. Abbiendi et al., Phys. Lett. B 559 (2003) 131.

[7] OPAL Coll., R. Akers et al., Z. Phys. C 67 (1995) 389;
DELPHI Coll., P. Abreu et al., Phys. Lett. B 379 (1996) 330;
OPAL Coll., G. Abbiendi et al., Eur. Phys. J. C 21 (2001) 23.

[8] OPAL Coll., K. Ackerstaff et al., Eur. Phys. J. C 5 (1998) 239.

[9] OPAL Coll., G. Abbiendi et al., Phys. Lett. B 523 (2001) 35.

[10] OPAL Coll., G. Abbiendi et al., Eur. Phys. J. C 16 (2000) 423.

[11] L3 Coll., M. Acciarri et al., Phys. Lett. B 458 (1999) 517;
DELPHI Coll., P. Abreu et al., Phys. Lett. B 471 (2000) 460;
ALEPH Coll., D. Abbaneo et al., Eur. Phys. J. C 36 (2004) 147.

[12] L3 Coll., P. Achard et al., Phys. Lett. B 547 (2002) 139;
OPAL Coll., G. Abbiendi et al., Eur. Phys. J. C 36 (2004) 297;
ALEPH Coll., D. Abbaneo et al., Phys. Lett. B 606 (2005) 265;
DELPHI Coll., J. Abdallah et al., Eur. Phys. J. C 44 (2005) 161.

[13] U. Heinz, Nucl. Phys. A 610 (1996) 264.

[14] U. Wiedemann, P. Scotto and U. Heinz, Phys. Rev. C 53 (1996) 918.

[15] Z. Chajecki (STAR Coll.), Nucl. Phys. A 774 (2006) 599.

[16] M.G. Bowler, Z. Phys. C 29 (1985) 617;
B. Andersson and W. Hofmann, Phys. Lett. B 169 (1986) 364;
U. Heinz and B.V. Jacak, Ann. Rev. Nucl. Part. Sci. 49 (1999) 529;
K. Geiger et al., Phys. Rev. D 61 (2000) 054002.

[17] G. Alexander, Phys. Lett. B 506 (2001) 45;
G. Alexander, Rept. Prog. Phys. 66 (2003) 481.

[18] T. Csörgő and J. Zimanyi, Nucl. Phys. A 517 (1990) 588;
A. Bialas et al., Phys. Rev. D 62 (2000) 114007;
A. Bialas et al., Acta Physica Polonica B 32 (2001) 2901.

[19] OPAL Coll., K. Ahmet et al., Nucl. Instr. and Methods A 305 (1991) 275.

[20] P.P. Allport et al., Nucl. Instr. and Methods A 324 (1993) 34; Nucl. Instr. and Methods A 346 (1994) 476.

[21] T. Csörgő and S. Pratt, Proc. Workshop on Relativistic Heavy Ion Physics at Present and Future Accelerators, eds. T. Csörgő et al., KFKI-1991-28/A, (KFKI, Budapest, 1991), p. 75.

[22] S. Chapman, P. Scotto and U. Heinz, Phys. Rev. Lett. 74 (1995) 4400.

[23] T. Sjöstrand, Comp. Phys. Comm. 39 (1986) 347;
T. Sjöstrand and M. Bengtsson, Comp. Phys. Comm. 43 (1987) 367; Comp. Phys. Comm. 82 (1994) 74.

[24] J. Allison et al., Nucl. Instr. and Methods A 317 (1992) 47.

[25] OPAL Coll., G. Alexander et al., Z. Phys. C 69 (1996) 543.

[26] S. Pratt, Phys. Rev. D 33 (1986) 1314;
G. Bertsch, M. Gong and M. Tohyama, Phys. Rev. C 37 (1988) 1896.

[27] F. Yano and S. Koonin, Phys. Lett. B 78 (1978) 556;
M.I. Podgoretsky, Sov. J. Nucl. Phys. 37 (1983) 272;
S. Chapman, J. Rayford Nix and U. Heinz, Phys. Rev. C 52 (1995) 2694.

[28] B. Tomasik and U. Heinz, Acta Physica Slovaca 49 (1999) 251;
K. Morita et al., Phys. Rev. C 61 (2000) 034904.

[29] F. James, CERN Program Library Long Writeup D506, CERN, 1994.

[30] GIBS Coll., M.Kh. Anikina et al., Phys. Lett. B 397 (1997) 30;
M.Kh. Anikina et al., Phys. Atom. Nucl. 67 (2004) 406.

[31] M. Gyulassy et al., Phys. Rev. C 20 (1979) 2267.

[32] T. Csörgő and S. Hegyi, Phys. Lett. B 489 (2000) 15.

[33] E-802 Coll., L. Ahle et al., Phys. Rev. C 66 (2002) 054906.

[34] U.A. Wiedemann and U. Heinz, Phys. Rev. C 56 (1997) 3265.

[35] S. Catani et al., Phys. Lett. B 269 (1991) 432.

[36] H. Heiselberg and A.P. Vischer, Eur. Phys. J. C 1 (1998) 593.

[37] STAR Coll., C. Adler et al., Phys. Rev. Lett. 87 (2001) 082301;
PHENIX Coll., K. Adcox et al., Phys. Rev. Lett. 88 (2002) 192302.

0.0 jY j< 0.8	0.1 k_t < 0.2 GeV	0.2 k_t < 0.3 GeV	0.3 k_t < 0.4 GeV	0.4 k_t < 0.5 GeV	0.5 k_t < 0.6 GeV
N	0:974 0:003 0:057	0:996 0:004 0:042	1:011 0:004 0:040	1:003 0:007 0:040	1:016 0:009 0:052
	0:286 0:011 0:067	0:364 0:009 0:061	0:429 0:012 0:047	0:398 0:013 0:044	0:337 0:016 0:063
$R^2_{t_{out}}$ (fm ^{2})	0:60 0:07 0:18	0:36 0:03 0:10	0:294 0:020 0:079	0:174 0:013 0:050	0:169 0:014 0:051
$R^2_{t_{side}}$ (fm ^{2})	0:50 0:03 0:14	0:38 0:02 0:11	0:37 0:02 0:11	0:30 0:02 0:10	0:22 0:03 0:10
R^2_{long} (fm ^{2})	1:09 0:11 0:37	0:72 0:04 0:17	0:82 0:05 0:16	0:60 0:04 0:15	0:75 0:06 0:18
$R^2_{long;t_{out}}$ (fm ^{2})	0:06 0:08 0:14	0:020 0:036 0:037	0:065 0:028 0:031	0:023 0:022 0:007	0:121 0:024 0:065
$_{t_{out}}$ (GeV ^{1})	0:091 0:004 0:060	0:056 0:004 0:035	0:037 0:004 0:027	0:016 0:005 0:018	0:003 0:006 0:018
$_{t_{side}}$ (GeV ^{1})	0:123 0:004 0:071	0:130 0:004 0:061	0:140 0:004 0:071	0:18 0:01 0:10	0:24 0:01 0:13
$_{long}$ (GeV ^{1})	0:081 0:004 0:023	0:048 0:004 0:017	0:019 0:005 0:015	0:016 0:007 0:019	0:018 0:008 0:038
^{2}/DoF	16389=15617	16080=15617	15596=15617	15864=15617	15439=15617
0.8 jY j< 1.6					
N	0:972 0:003 0:049	0:990 0:004 0:075	1:017 0:005 0:052	1:019 0:007 0:057	1:024 0:010 0:066
	0:315 0:008 0:070	0:386 0:008 0:064	0:393 0:011 0:053	0:379 0:013 0:055	0:318 0:016 0:062
$R^2_{t_{out}}$ (fm ^{2})	0:62 0:04 0:20	0:38 0:02 0:11	0:271 0:016 0:079	0:204 0:014 0:062	0:141 0:015 0:053
$R^2_{t_{side}}$ (fm ^{2})	0:52 0:03 0:13	0:38 0:02 0:11	0:34 0:02 0:10	0:272 0:021 0:081	0:226 0:026 0:079
R^2_{long} (fm ^{2})	1:06 0:08 0:35	0:71 0:04 0:16	0:65 0:04 0:15	0:64 0:05 0:16	0:50 0:05 0:12
$R^2_{long;t_{out}}$ (fm ^{2})	0:019 0:055 0:076	0:029 0:026 0:036	0:036 0:023 0:025	0:061 0:022 0:045	0:034 0:021 0:042
$_{t_{out}}$ (GeV ^{1})	0:070 0:004 0:049	0:046 0:004 0:035	0:033 0:004 0:033	0:015 0:005 0:027	0:007 0:007 0:009
$_{t_{side}}$ (GeV ^{1})	0:106 0:004 0:059	0:104 0:004 0:051	0:131 0:005 0:064	0:161 0:005 0:088	0:23 0:01 0:14
$_{long}$ (GeV ^{1})	0:066 0:004 0:026	0:035 0:004 0:026	0:003 0:005 0:036	0:028 0:006 0:047	0:060 0:009 0:072
^{2}/DoF	15856=15617	15745=15617	15658=15617	15895=15617	15592=15617
1.6 jY j< 2.4					
N	0:991 0:003 0:082	1:019 0:005 0:069	1:066 0:005 0:078	1:055 0:008 0:074	1:07 0:01 0:10
	0:261 0:008 0:079	0:307 0:008 0:072	0:299 0:011 0:065	0:264 0:014 0:074	0:24 0:02 0:11
$R^2_{t_{out}}$ (fm ^{2})	0:54 0:04 0:19	0:35 0:02 0:11	0:35 0:03 0:10	0:219 0:017 0:064	0:25 0:03 0:11
$R^2_{t_{side}}$ (fm ^{2})	0:53 0:03 0:15	0:34 0:02 0:10	0:279 0:023 0:077	0:229 0:026 0:072	0:169 0:034 0:085
R^2_{long} (fm ^{2})	1:13 0:09 0:41	0:61 0:04 0:17	0:78 0:06 0:19	0:62 0:05 0:17	0:54 0:07 0:13
$R^2_{long;t_{out}}$ (fm ^{2})	0:05 0:05 0:13	0:012 0:029 0:033	0:137 0:033 0:076	0:148 0:024 0:077	0:09 0:04 0:11
$_{t_{out}}$ (GeV ^{1})	0:102 0:004 0:070	0:063 0:004 0:048	0:060 0:005 0:043	0:027 0:006 0:028	0:16 0:01 0:12
$_{t_{side}}$ (GeV ^{1})	0:134 0:004 0:079	0:130 0:004 0:068	0:167 0:005 0:082	0:19 0:01 0:11	0:31 0:01 0:17
$_{long}$ (GeV ^{1})	0:045 0:004 0:056	0:003 0:005 0:045	0:046 0:005 0:053	0:078 0:007 0:072	0:15 0:01 0:13
^{2}/DoF	15966=15617	15866=15617	15735=15617	15235=15617	15279=15617

Table 1: Results of the Bertsch-Pratt ts, Eq. (7), to the experimental three-dimensional correlation functions $C^0(Q_{\ell}; Q_{t_{side}}; Q_{t_{out}})$ over the range 0.04 $Q_{\ell}; Q_{t_{side}}; Q_{t_{out}}$ 1.0 GeV. The rst errors are statistical and the second systematic. The quality of the ts is indicated by the value of ^{2}/DoF, which ranges from 0.98 to 1.05.

$0.0 \le |Y| < 0.8$	$0.1 \le k_t < 0.2$ GeV	$0.2 \le k_t < 0.3$ GeV	$0.3 \le k_t < 0.4$ GeV	$0.4 \le k_t < 0.5$ GeV	$0.5 \le k_t < 0.6$ GeV
N	0.993 0.003 0.010	1.004 0.003 0.008	0.985 0.004 0.017	0.946 0.005 0.041	0.85 0.01 0.14
	0.266 0.012 0.067	0.358 0.009 0.056	0.441 0.012 0.035	0.440 0.013 0.023	0.482 0.017 0.069
v	0.10 0.19 0.32	0.288 0.042 0.018	0.320 0.030 0.013	0.249 0.034 0.010	0.211 0.031 0.031
R_0^2 (fm^2)	0.52 0.20 0.16	0.184 0.044 0.075	0.226 0.022 0.088	0.203 0.013 0.081	0.110 0.009 0.053
R_t^2 (fm^2)	0.75 0.04 0.17	0.50 0.02 0.12	0.41 0.02 0.10	0.313 0.011 0.081	0.193 0.007 0.048
R_ℓ^2 (fm^2)	1.15 0.15 0.34	0.74 0.04 0.13	0.66 0.03 0.11	0.46 0.02 0.10	0.31 0.02 0.11
$_0$ (GeV^{-1})	0.045 0.007 0.069	0.014 0.006 0.052	0.008 0.007 0.019	0.061 0.008 0.062	0.156 0.011 0.091
$_t$ (GeV^{-1})	0.099 0.004 0.029	0.089 0.005 0.023	0.065 0.006 0.030	0.066 0.008 0.036	0.054 0.013 0.019
$_\ell$ (GeV^{-1})	0.038 0.002 0.098	0.014 0.002 0.090	0.005 0.003 0.051	0.001 0.003 0.025	0.002 0.005 0.012
^{2}/DoF	13583/11677	16008/14375	17555/16338	18166/17554	18702/18232
$0.8 \le |Y| < 1.6$					
N	0.948 0.005 0.021	0.977 0.006 0.006	0.964 0.009 0.010	0.914 0.012 0.051	0.859 0.022 0.072
	0.324 0.008 0.065	0.380 0.010 0.057	0.425 0.013 0.035	0.464 0.019 0.023	0.464 0.034 0.028
v	0.754 0.022 0.061	0.782 0.014 0.036	0.742 0.017 0.027	0.777 0.014 0.031	0.743 0.023 0.040
R_0^2 (fm^2)	0.187 0.054 0.076	0.104 0.024 0.051	0.114 0.016 0.054	0.102 0.013 0.051	0.106 0.011 0.052
R_t^2 (fm^2)	0.56 0.02 0.15	0.39 0.01 0.11	0.32 0.01 0.10	0.235 0.010 0.071	0.164 0.009 0.049
R_ℓ^2 (fm^2)	0.83 0.06 0.27	0.58 0.03 0.13	0.46 0.03 0.10	0.43 0.03 0.12	0.294 0.032 0.085
$_0$ (GeV^{-1})	0.07 0.01 0.10	0.00 0.01 0.12	0.071 0.010 0.053	0.106 0.012 0.076	0.125 0.019 0.084
$_t$ (GeV^{-1})	0.068 0.007 0.041	0.075 0.008 0.033	0.069 0.011 0.043	0.046 0.015 0.036	0.079 0.027 0.079
$_\ell$ (GeV^{-1})	0.099 0.010 0.078	0.022 0.008 0.099	0.032 0.008 0.062	0.058 0.010 0.047	0.077 0.014 0.060
^{2}/DoF	8624/7139	9778/8788	11004/9870	11365/10518	11603/10885
$1.6 \le |Y| < 2.4$					
N	0.899 0.016 0.054	0.963 0.020 0.064	0.902 0.021 0.040	0.888 0.028 0.052	0.48 0.01 0.39
	0.342 0.019 0.078	0.354 0.022 0.072	0.454 0.012 0.041	0.438 0.038 0.030	1.26 0.04 0.63
v	0.893 0.012 0.044	0.931 0.008 0.047	0.927 0.009 0.033	0.912 0.012 0.042	0.93 0.04 0.11
R_0^2 (fm^2)	0.031 0.043 0.029	0.006 0.032 0.022	0.015 0.026 0.025	0.020 0.030 0.026	0.034 0.024 0.019
R_t^2 (fm^2)	0.39 0.02 0.12	0.291 0.017 0.087	0.172 0.011 0.052	0.159 0.014 0.048	0.071 0.005 0.021
R_ℓ^2 (fm^2)	0.42 0.05 0.16	0.42 0.05 0.15	0.34 0.03 0.10	0.38 0.06 0.10	0.12 0.03 0.11
$_0$ (GeV^{-1})	0.03 0.04 0.12	0.060 0.029 0.080	0.014 0.033 0.021	0.196 0.031 0.075	0.00 0.03 0.16
$_t$ (GeV^{-1})	0.033 0.023 0.082	0.087 0.024 0.093	0.030 0.009 0.050	0.070 0.032 0.055	0.216 0.031 0.071
$_\ell$ (GeV^{-1})	0.001 0.036 0.066	0.049 0.028 0.081	0.025 0.030 0.054	0.162 0.029 0.065	0.02 0.03 0.16
^{2}/DoF	4168/3804	5110/4648	5952/5169	5775/5490	5876/5642

Table 2: Results of the Yano-Koonin fits, Eq. (8), to the experimental three-dimensional correlation functions $C'(q_t, q_\ell, q_0)$ over the range $0.04 \le q_t, q_\ell, q_0 \le 1.0$ GeV. The first errors are statistical and the second systematic. The quality of the fits is indicated by the value of ^{2}/DoF, which ranges from 1.03 to 1.20.

	BP radii		YK radii	
	dR^2_{long}/dk_t (fm^2/GeV)	$dR^2_{t_{side}}/dk_t$ (fm^2/GeV)	$dR^2_{\parallel}/dk_t$ (fm^2/GeV)	$dR^2_{\perp}/dk_t$ (fm^2/GeV)
$\lvert Y\rvert < 0.8$	$0.46 \pm 0.20 \pm 0.35$	$0.59 \pm 0.08 \pm 0.19$	$1.60 \pm 0.13 \pm 0.38$	$1.14 \pm 0.05 \pm 0.23$
$0.8 \leq \lvert Y\rvert < 1.6$	$0.91 \pm 0.18 \pm 0.30$	$0.66 \pm 0.08 \pm 0.15$	$1.04 \pm 0.12 \pm 0.23$	$0.84 \pm 0.04 \pm 0.15$
$1.6 \leq \lvert Y\rvert < 2.4$	$0.64 \pm 0.21 \pm 0.36$	$0.80 \pm 0.09 \pm 0.28$	$0.82 \pm 0.13 \pm 0.17$	$0.70 \pm 0.04 \pm 0.20$

Table 3: Slopes of the linear fits to the dependence of the longitudinal and transverse squared radii of the BP and YK parameterizations on k_t. Input to the fits are the measured values of R^2_{long}, $R^2_{t_{side}}$, $R^2_{\parallel}$ and $R^2_{\perp}$, reported in Tables 1 and 2. The first errors are statistical and the second systematic.